BULLETIN OF THE POLISH ACADEMY OF SCIENCES
TECHNICAL SCIENCES, Vol. 63, No. 3, 2015
DOI: 10.1515/bpasts-2015-0070

Comparative analysis of GaAs- and GaSb-based active regions emitting in the mid-infrared wavelength range

Ł. PISKORSKI*, L. FRASUNKIEWICZ, and R.P. SARZAŁA

Photonics Group, Institute of Physics, Lodz University of Technology, 219 Wolczanska St., 90-924 Lodz, Poland

Abstract. In the present paper the results of the computer analysis of the GaAs-based and GaSb-based active regions that can be applied in compact semiconductor laser sources of radiation at mid-infrared wavelengths are presented. Quantum well material contents and strain dependencies on the maximal gain are investigated. It is shown that above 3 μm the maximal gain obtained for GaInNAs/AlGaInAs active region is high only for thick, highly-strained GaInNAs QWs with N concentration higher than 2%. Much higher gain in this wavelength range can be obtained for GaInAsSb/AlGaAsSb active region, which offers relatively high gain even at 4.5 μm when the Sb content in GaInAsSb and compressive strain in this layer are equal to 50% and – 2%, respectively.

Key words: strained QWs, GaInNAs, GaInAsSb, mid-infrared radiation, numerical analysis.

1. Introduction

Currently, there is considerable interest in mid-infrared semiconductor lasers operating in the room-temperature (RT) continuous-wave (CW) regime due to their possible applications in wireless optical communication, medical diagnostics, thermovision measurements, distant air monitoring. In the case of the latter, until recently, various gas-sensing systems mainly based on electrochemical sensors have been used. However, they suffer from slow response times and ageing, when used in corrosive gas atmospheres. An alternative here is tunable-diode-laser-absorption-spectroscopy (TDLAS) – a rapid and contactless technique for gas detection [1–3] which uses a laser device to scan the wavelength range of several nanometres. For such a system only compact electrically-pumped single-mode RT-CW operating laser sources are particularly suitable, for which it is possible to tune the wavelength over few nanometres around the desired wavelength without mode-hopping [1]. Two candidates can be considered for this application: DFBs (distributed feed-back lasers) and VCSELs. For TDLAS, mostly DFBs have been applied so far. However, these devices have high power consumption, limited tuning range and slow scanning speed, compared to VCSELs which have a low cost potential, the ability to be modulated at very high frequencies, and in-situ testing possibility. Small volume of the lasing material in VCSELs means that their emission wavelength can be very rapidly current-tuned over ranges exceeding 1 nm, which allows several absorption transitions to be covered in a single wavelength scan [4, 5]. Furthermore, for micro-electro-mechanical-system VCSELs where the cavity can be tuned by an electro-thermal actuation of the MEMS mirror [6], it is possible to achieve continuous tuning range close to 50 nm [7].

Although there are several important gases, like C_2O, N_20, H_2S, CH_4 (see Fig. 1), in the mid-infrared spectral range, the longest wavelength reported to date for electrically pumped RT CW VCSELs is 2.62 μm [8, 9]. Shifting this wavelength further into the infrared is extremely difficult due to well-known strong non-radiative Auger recombination effect and high free carrier absorption at long wavelengths (see Fig. 2). Although these mechanisms cannot be completely eliminated, it is still possible to reduce them, and therefore to increase the laser performance. One of possible solutions in this field is to make an optimal design of the VCSEL active region by selecting the material contents for quantum wells (QWs) and barriers. Due to relation between the material content of the layer and strain in this layer it is important to take some limitations into account. One of them is the critical thickness of the layer h_c which can be easily estimated when the strain ε is known [10, 11]:

$$h_c = \left(\frac{16}{|\varepsilon|}\right)^{2.4}, \tag{1}$$

where units of strain and critical thickness in this relation are % and Å, respectively.

In the case of multi quantum well active region with strained QWs the average strain can limit the number of active layers. To overcome this problem the strain with opposite sign is introduced into the barriers. This solution enables the use of multi quantum well active region even with thick (∼10 nm) QWs. However, the crucial issue remains the combination of the material contents and layers widths that is able to provide both low average strain and high optical gain. An efficient way to investigate it is to apply a computer simulation of strain effects and optical gain in multi quantum well active region. In this work the results of such simulation will be presented for arsenide-based (GaInNAs/AlGaInAs) and antimonide-based (GaInAsSb/AlGaAsSb) active regions for which, as shown in Fig. 3, it is possible to obtain laser light in the mid-infrared range.

*e-mail: lukasz.piskorski@p.lodz.pl

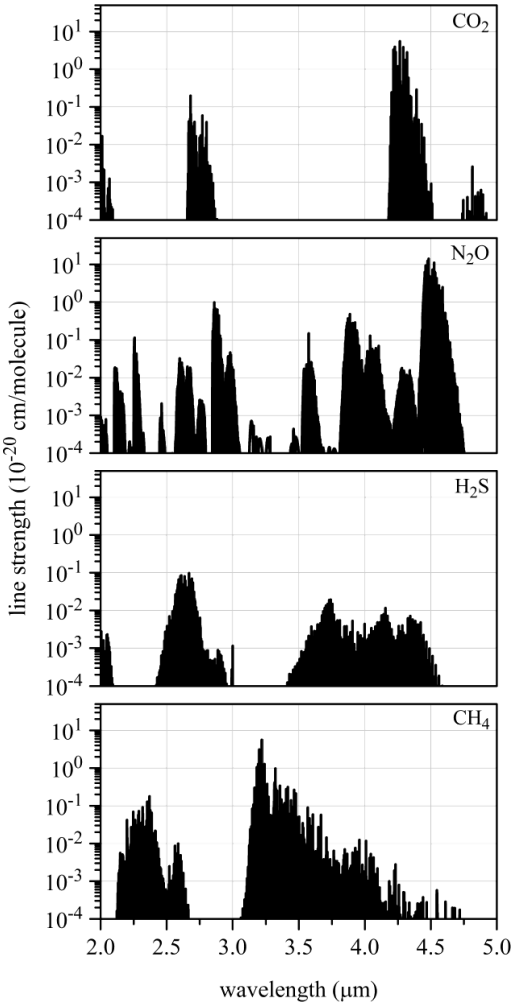

Fig. 1. Absorption lines of CO_2, N_2O, H_2S and CH_4 and as a function of wavelength, in the spectral range from 2 to 5 μm. Data taken from Ref. 8

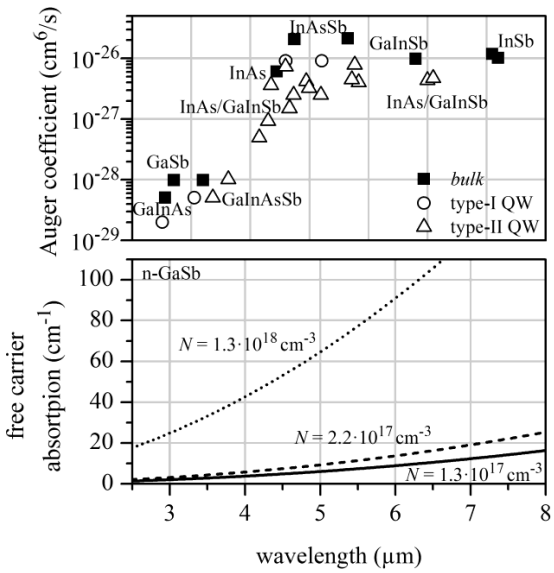

Fig. 2. Wavelength dependences of Auger coefficient (top) and free carrier absorption (bottom) for selected antimonides after Ref. 10

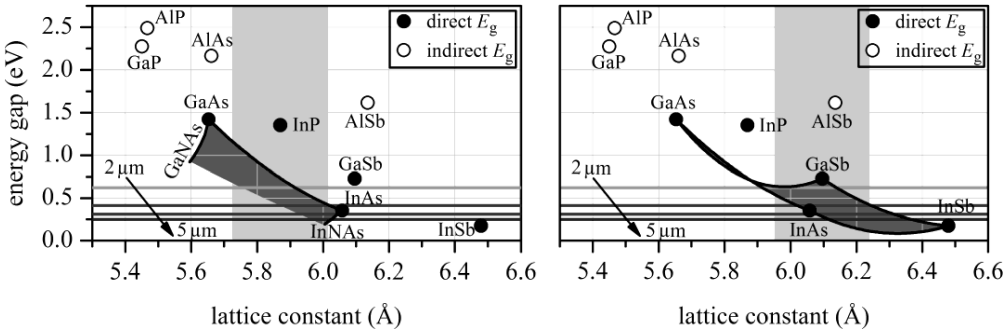

Fig. 3. Energy gap as a function of lattice constant for GaInNAs (left) and GaInAsSb (right). The mid-infrared region of the spectrum has been shown with the use of horizontal lines corresponding to wavelengths from 2 μm to 5 μm

2. The model

We used a numerical model which allows a prediction of the conduction- and valence-band shifts caused by the lattice mismatch between active region and substrate. This model extends a previous model used by authors in [12] which was valid only for unstrained barriers. To realize thick active region with multiple strained quantum wells the average strain in the active region must be close to zero. To fulfil this condition barriers must provide a strain compensation (strain in barrier layers must be of equal magnitude but opposite sign to strain provided by quantum wells).

Using approach given in [13] strains in the active region layers can be determined with the aid of:

$$\varepsilon^{\mathrm{w(b)}} = \frac{a_{\mathrm{lc}}^{\mathrm{sub}} - a_{\mathrm{lc}}^{\mathrm{w(b)}}}{a_{\mathrm{lc}}^{\mathrm{w(b)}}}, \tag{2}$$

where $\varepsilon^{\mathrm{w(b)}}$ – strain in the quantum (barrier), $a_{\mathrm{lc}}^{\mathrm{sub}}$ – substrate lattice constant, $a_{\mathrm{lc}}^{\mathrm{w(b)}}$ – quantum well (barrier) lattice constant. For strained active region the conduction- and valence-band edges are shifted and the valence band is further split into heavy-hole and light-hole subbands:

$$E_{\mathrm{c}}^{\mathrm{w(b)}} = E_{\mathrm{c},0}^{\mathrm{w(b)}} + \Delta E_{\mathrm{c}}^{\mathrm{w(b)}}, \tag{3}$$

$$E_{\mathrm{v,hh}}^{\mathrm{w(b)}} = E_{\mathrm{v},0}^{\mathrm{w(b)}} + \Delta E_{\mathrm{v,hh}}^{\mathrm{w(b)}}, \tag{4}$$

$$E_{\mathrm{v,lh}}^{\mathrm{w(b)}} = E_{\mathrm{v},0}^{\mathrm{w(b)}} + \Delta E_{\mathrm{v,lh}}^{\mathrm{w(b)}}. \tag{5}$$

Symbols from (3)–(5) are explained in Fig. 4 which illustrates energy-band diagrams for active regions with different combinations of strain values in quantum wells and barrier layers.

The conduction band experiences a shift due to the hydrostatic component:

$$\Delta E_{\mathrm{c}}^{\mathrm{w(b)}} = \Delta E_{\mathrm{c,hy}}^{\mathrm{w(b)}}, \tag{6}$$

whereas for valence band both hydrostatic and shear components should be taken into account:

$$\Delta E_{\mathrm{v,hh}}^{\mathrm{w(b)}} = \Delta E_{\mathrm{v,hy}}^{\mathrm{w(b)}} + \Delta E_{\mathrm{v,hh,sh}}^{\mathrm{w(b)}}, \tag{7}$$

$$\Delta E_{\mathrm{v,lh}}^{\mathrm{w(b)}} = \Delta E_{\mathrm{v,hy}}^{\mathrm{w(b)}} + \Delta E_{\mathrm{v,lh,sh}}^{\mathrm{w(b)}}, \tag{8}$$

where, for active region grown along the [001] direction:

$$\Delta E_{\mathrm{c,hy}}^{\mathrm{w(b)}} = 2a_{\mathrm{c}}^{\mathrm{w(b)}} \left(1 - \frac{c_{12}^{\mathrm{w(b)}}}{c_{11}^{\mathrm{w(b)}}}\right) \varepsilon^{\mathrm{w(b)}}, \tag{9}$$

$$\Delta E_{\mathrm{v,hy}}^{\mathrm{w(b)}} = 2a_{\mathrm{v}}^{\mathrm{w(b)}} \left(1 - \frac{c_{12}^{\mathrm{w(b)}}}{c_{11}^{\mathrm{w(b)}}}\right) \varepsilon^{\mathrm{w(b)}}, \tag{10}$$

$$\Delta E_{\mathrm{hh,sh}}^{\mathrm{w(b)}} = -\frac{1}{2}\Delta E_{\mathrm{sh}}^{\mathrm{w(b)}}, \tag{11}$$

$$\Delta E_{\mathrm{lh,sh}}^{\mathrm{w(b)}} = -\frac{1}{2}\Delta_{\mathrm{so}}^{\mathrm{w(b)}} + \frac{1}{4}\Delta E_{\mathrm{sh}}^{\mathrm{w(b)}} + \frac{1}{2}\sqrt{\left(\Delta_{\mathrm{so}}^{\mathrm{w(b)}}\right)^2 + \Delta_{\mathrm{so}}^{\mathrm{w(b)}}\Delta E_{\mathrm{sh}}^{\mathrm{w(b)}} + \frac{9}{4}\left(\Delta E_{\mathrm{sh}}^{\mathrm{w(b)}}\right)^2}, \tag{12}$$

$$\Delta E_{\mathrm{sh}}^{\mathrm{w(b)}} = -2b^{\mathrm{w(b)}} \left(1 + \frac{c_{12}^{\mathrm{w(b)}}}{c_{11}^{\mathrm{w(b)}}}\right) \varepsilon^{\mathrm{w(b)}}. \tag{13}$$

where $a_{\mathrm{c}}^{\mathrm{w(b)}}$, $a_{\mathrm{v}}^{\mathrm{w(b)}}$, $b^{\mathrm{w(b)}}$ – deformation potentials, $c_{11}^{\mathrm{w(b)}} c_{12}^{\mathrm{w(b)}}$ – elastic constants, $\Delta_{\mathrm{so}}^{\mathrm{w(b)}}$ – split-off energy. To calculate the above parameters for active region materials ($A_xB_{1-x}C_yD_{1-y}$ or $A_xB_yC_zD$) the nonlinear interpolation schemes [14] using the binary values B [15, 16] for III–V materials and bowing parameters C [15] have been used:

$$\begin{aligned} Q_{ABCD} = {} & xyB_{AC} + x(1-y)B_{AD} + (1-x)yB_{BC} \\ & + (1-x)(1-y)B_{BD} - x(1-x)yC_{ABC} \\ & - x(1-x)(1-y)C_{ABD} - xy(1-y)C_{ACD} \\ & - (1-x)y(1-y)C_{BCD} - x(1-x)y(1-y)C_{ABCD}, \end{aligned} \tag{14}$$

$$\begin{aligned} Q_{ABCD} = {} & xB_{AD} + yB_{BD} + zB_{CD} - xyC_{ABD} \\ & - yzC_{BCD} - xzC_{ACD} - xyzC_{ABCD}. \end{aligned} \tag{15}$$

It is worthy to mention that equations (14) and (15) can be easily extended for quinary materials, for example GaInNAsSb or AlGaInAsSb, which will ensure that this work results will be compatible with those which can be used in further study.

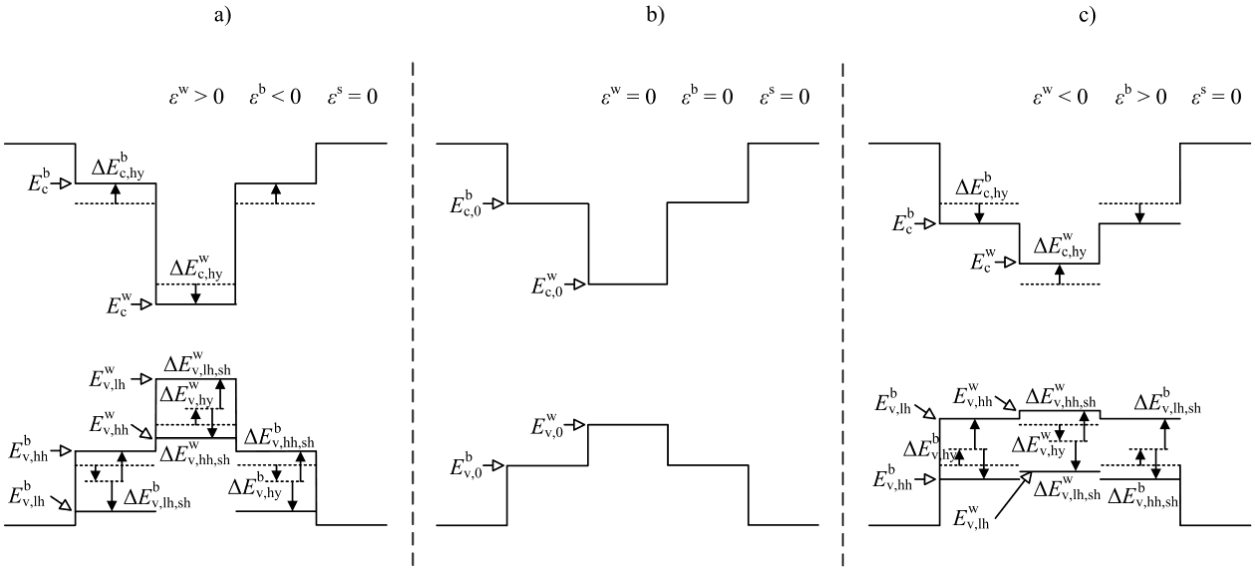

Fig. 4. Band diagrams of the active regions with strained quantum wells and barriers and lattice-matched to substrate spacers together with the conduction- and valence-band shifts

In the calculation of the optical gain, the classical Fermi's golden rule [17] and the parabolic band-gap approximation are assumed [18, 19]. The optical gain spectra g may then be determined from the following relation:

$$g(\hbar\omega) = \sum_m \int_{-\infty}^{+\infty} g_m(\varepsilon)\,\Lambda(\hbar\omega - \varepsilon)\,\mathrm{d}\varepsilon \tag{16}$$

where the summation should be carried out over all available numbers m of level pairs and

$$g_m(\hbar\omega) = \frac{\pi\rho^{2\mathrm{D}}(\hbar\omega)\,|M|^2\,e^2}{cn_{\mathrm{R}}m_0^2\varepsilon_0\omega} \cdot \{f_{\mathrm{c}}[E_{\mathrm{e}}(m,\hbar\omega)] - f_{\mathrm{v}}[E_{\mathrm{h}}(m,\hbar\omega)]\}, \tag{17}$$

where n_{R} stands for the index of refraction, c is the speed of light in vacuum, m_0 is the free electron mass, ε_0 is the vacuum dielectric constant, M is the momentum matrix element calculated from the Kane model [20], $\rho^{2\mathrm{D}}$ stands for the two-dimensional reduced density of states, f_{c} and f_{v} are the Fermi-Dirac functions determined for electrons in the conduction band and for holes in the valence band, respectively, E_{e} and E_{h} are the energies of the recombining electron and hole, respectively, and Λ is the broadening function [21], usually of Lorentzian type.

Gain parameters used in calculations were estimated from their values for binaries given in [11, 15, 16] using interpolation formulas (14) and (15) and bowing parameters taken from [11, 15]. Only two exceptions from this procedure were introduced in order to give better agreement with experimental results in the case of GaInNAs energy gap and electron effective mass. Further details of the calculation of these two parameters can be found in [12, 22].

3. The results

The optimal active-region structure is expected to ensure low-threshold room-temperature emission of the radiation of the desired wavelength, in this case in the range above 2.62 μm, which is still not accessible for VCSELs. In this section, two different QW material systems will be considered for which it is possible to obtain laser light in the mid-infrared range: GaInNAs/AlGaInAs on InP (to the best of our knowledge only theoretical studies were conducted for these active regions [12, 23–25]) and GaInAsSb/AlGaAsSb on GaSb. An impact of parameters such as nitrogen/antimony content, strain, thickness of these QWs is to be investigated. Contrary to our previous paper [26], the gain spectra are presented both for low and high Al contents in barrier layers.

At first, let us consider the unstrained ($\varepsilon^{\mathrm{w}} = 0\%$) GaInNAs/AlGaInAs active region (Fig. 5a) with 8-nm thick QW at room-temperature (300 K). As can be seen, for the QW carrier concentration of $3{\cdot}10^{18}$ cm^{-3} which should be achievable in mid-infrared VCSELs [25, 27], irrespective of nitrogen content in QW and aluminium content in barriers, the positive gain is not available in this QW for wavelength values higher

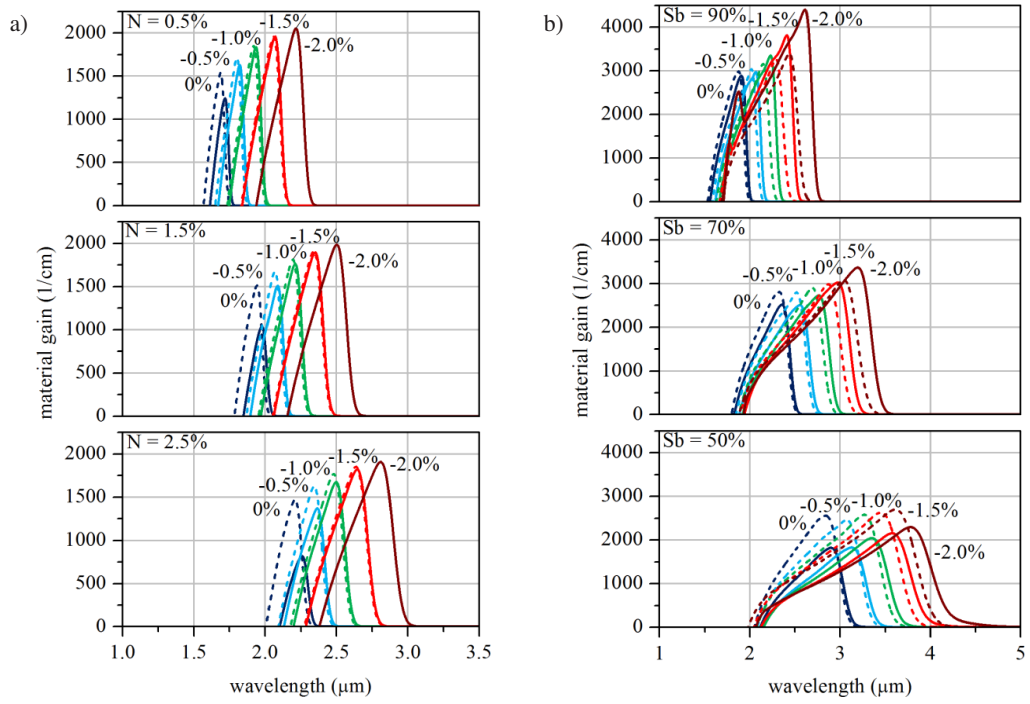

Fig. 5. Gain spectra calculated for a) GaInNAs/AlGaInAs and b) GaInAsSb/AlGaAsSb active regions at various strains and nitride (antimonide) contents with $T = 300$ K and $n^{\mathrm{w}} = 3 \cdot 10^{18}$ cm^{-3}. Solid lines correspond to the active regions with Al content in barrier layers equal to 10%, whereas dashed ones to the highest possible Al content in these layers which is able to provide I-type QW with direct energy gap barrier (maximal Al content was equal to 50%). In each case quantum well and barrier widths were equal to 8 nm and 5 nm, respectively, and strains in these layers had the same absolute value but opposite sign. Values of the compressive strain in QW are additionally shown

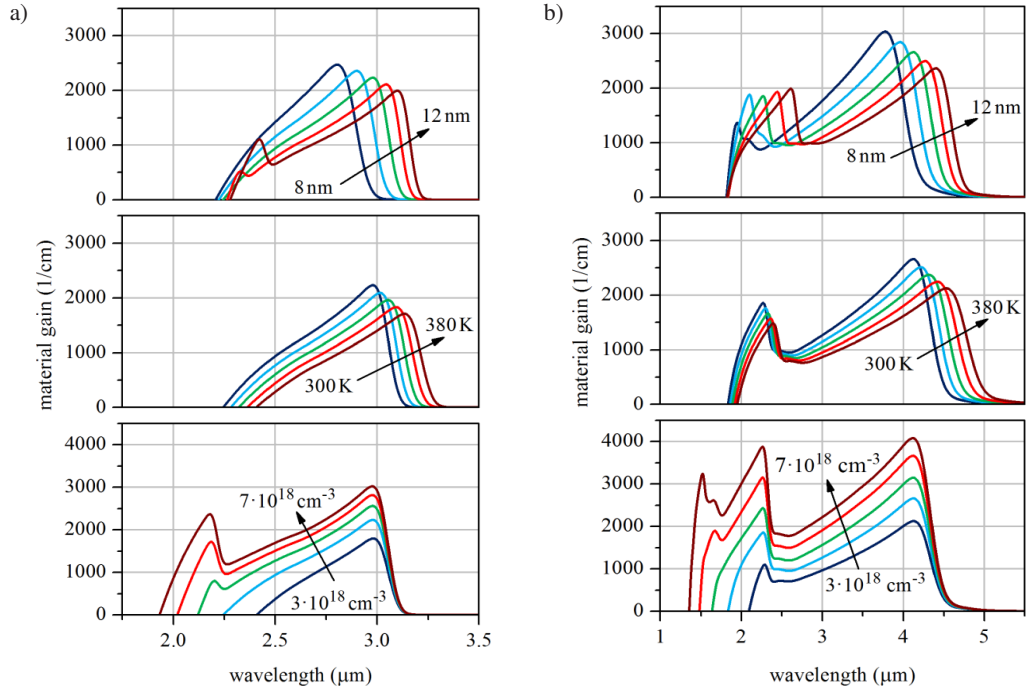

Fig. 6. Gain spectra calculated for
a) $Ga_{0.10}In_{0.90}N_{0.025}As_{0.975}/Al_{0.10}Ga_{0.65}In_{0.25}As$ and b) $Ga_{0.34}In_{0.66}As_{0.50}Sb_{0.50}/Al_{0.10}Ga_{0.90}As_{0.28}Sb_{0.72}$
active regions at various quantum well widths (top), temperatures (centre) and carrier concentrations (bottom) with $\varepsilon^{w} = -2\%$ and $\varepsilon^{b} = 2\%$. $T = 300$ K, $n^{w} = 4 \cdot 10^{18}$ cm^{-3}, $d^{w} = 10$ nm, $d^{b} = 5$ nm (unless otherwise stated)

than about 2.4 μm. Although gain spectra can be shifted towards longer wavelengths by increasing the compressive strain in the QW (to increase the strain for a given N content in GaInNAs, indium content must be increased), for $N = 0.5\%$, even for highly-strained QW ($\varepsilon^{w} = -2\%$), it is still not possible to observe positive gain in the desired wavelength range. It is shown that only the combination of high strain in the QW ($\varepsilon^{w} = -2\%$) and high nitrogen content ($N = 2.5\%$) in this layer leads to acceptable gain value of almost 2000 cm^{-1} for 2.8 μm. However, for wavelengths longer than 3 μm, gain values are again close to 0.

An additional red shift of gain spectra may be expected for active regions with thicker QWs. Room-temperature gain spectra determined for GaInNAs/AlGaInAs QW structure with $\varepsilon^{w} = -2\%$ and $N = 2.5\%$ and QW widths from 8–12 nm range are plotted in Fig. 6a (top). As compared with analogous spectra plotted in Fig. 5a (bottom), the spectra determined for wider QWs are red shifted – up to 0.25 μm for 12-nm thick QW. From Fig. 6a (centre) it can be seen that gain spectra shift toward longer wavelengths also due to temperature increment, however, as in the case of increasing the QW thickness, the maximal gain value is distinctly decreasing. To overcome the drop in maximal gain value, the solutions leading to the increment of the carrier concentration, Fig. 6a (bottom), in the active region may be necessary, nevertheless it is very difficult to increase the carrier concentration in VCSEL active region without deteriorating the performance characteristics of the device. Taking into account all the above results together with a undesired blue shift induced by annealing (which reduces the density of defects in the structure), it is seen that the maximal achievable wavelength for arsenide-based active region grown on InP is about 3 μm.

To obtain longer wavelength from III–V QWs, antimonide-based materials should be used. Compressive strain in GaInAsSb for a given Sb content is proportional to the amount of indium incorporated into this material. For highly-strained active layers the calculated gain is as high as 4000 cm^{-1} even for carrier concentration of $3{\cdot}10^{18}$ cm^{-3} for wavelengths below 3 μm (Fig. 5b (top)) at RT. With an antimony concentration in QW of 70% or 50% it is possible to obtain gain values higher than 3000 cm^{-1} for 3.2 μm (Fig. 5b (centre)) and 2000 cm^{-1} for 3.8 μm (Fig. 5b (bottom)), respectively. From Fig. 5b (bottom) it can be seen that even for unstrained GaInAsSb/AlGaAsSb active region the calculated gain is higher than for optimal GaInNAs/AlGaInAs one.

As in the case of arsenide-based active layers, the gain spectrum for antimonide-based active region can be shifted further into the longer wavelengths by using the thicker QW, Fig. 6b (top), or for higher temperatures, Fig. 6b (centre). For 12-nm thick GaInAsSb QW the wavelength corresponding to the peak of gain is close to 4.4 μm. Similar value (4.5 μm) was obtained for 8-nm QW in 380 K. While shifts in gain peak versus QW thickness and temperature have similar values compared to arsenide-based QW, the change of carrier concentration leads to much greater changes in gain value. As can be seen from Fig. 6b (bottom) by increasing the carrier concentration in GaInAsSb/AlGaAsSb active region from

$3{\cdot}10^{18}$ cm^{-3} to $7{\cdot}10^{18}$ cm^{-3} it is possible to achieve maximal gain higher by about 2000 cm^{-1} which is about two times higher than for GaInNAs/AlGaInAs active region. However, results obtained for high carrier concentrations in QW should be treated with some caution as there is some doubt whether such concentrations can be achieved. Although even higher carrier concentrations were reported for numerically simulated infrared VCSELs [28] (up to $1.1{\cdot}10^{19}$ cm^{-3} for devices with tunnel-junction diameter of 4 μm), for mid-infrared emission wavelengths the maximal carrier concentrations are expected to be lower, mainly due to small band discontinuities caused by band-edge shifts (Fig. 4c). Nevertheless, it seems that active regions based on antimonides are the best choice for use in mid-infrared VCSELs, even if we take into consideration blue shift of 60 meV [29] which is typical for antimonide-based QWs. Moreover, GaInAsSb/AlGaAsSb QWs can be further optimized, for example, by adding indium into the AlGaAsSb barriers to improve the hole confinement.

The numerical model together with the results presented above may be useful in designing of the active region for the mid-infrared semiconductor lasers able to operate in the selected wavelength range of several nanometres. Especially for wavelengths above 2.62 μm, where, to our knowledge, no RT CW has been reported for VCSELs, it is important to determine the optimal QW structural and material parameters for which the possible emission wavelength will correspond to the gain peak at the given ambient temperature. Although the determination of optimal parameters describing the active region does not imply that the device will achieve RT CW operation, it is still one of the main issue in achieving this goal.

4. Conclusions

We have used the comprehensive computer simulation to determine gain spectra for arsenide-based (GaInNAs/AlGaInAs) and antimonide-based (GaInAsSb/AlGaAsSb) active regions in the mid-infrared wavelength range. The influence of material contents, thicknesses and strains both in quantum well and barriers on the maximal gain are investigated. We found that the maximal achievable wavelength for arsenide-based active region grown on InP is about 3 μm and it can be obtain only for thick, highly-strained GaInNAs QWs with nitrogen concentration higher than 2%. To design a semiconductor laser based on III-V materials emitting in the wavelength range above 3 μm an antimonide-based active region should be used. It offers relatively high gain even at 4.5 μm when the antimony content in GaInAsSb and compressive strain in this layer are equal to 50% and -2%, respectively.

Acknowledgements. This work has been supported by the Polish National Science Centre (DEC-2012/07/D/ST7/02581).

REFERENCES

[1] A. Vicet, D. A. Yarekha, A. Perona, Y. Rouillard, S. Gaillard, and A.N. Baranov, "Trace gas detection with antimonide-based quantum-well diode lasers", *Spectrochim. Acta* A 58 (11), 2405–2412 (2002).

[2] P. Werle, "A review of recent advances in semiconductor laser based gas monitors", *Spectrochim. Acta* A 54 (2), 197–236 (1998).

[3] P. Werle, F. Slemr, K. Maurer, R. Kormann, R. Mucke, and B. Janker, "Near- and mid-infrared laser-optical sensors for gas analysis", *Opt. Las. Eng.* 37 (2–3), 101–114 (2002).

[4] L.C. Webster, S. O'Byrne, and A.F.P. Houwing "Determination of temperature distributions in air using a scanning vertical-cavity surface-emitting laser", *Fourth Australian Conf. Laser Diagnostics in Fluid Mechanics and Combustion* 1, 141–144 (2005).

[5] G. Overton, "VCSELs benefit TDLAS combustion measurements", *Laser Focus World* 49 (10), 13 (2013).

[6] S. Schilt, K. Zogal, B. Kögel, P. Meissner, M. Maute, R. Protasio, and M.-C. Amann, "Spectral and modulation properties of a largely tunable MEMS-VCSEL in view of gas phase spectroscopy applications", *Appl. Phys.* B 100 (2), 321–329 (2010).

[7] T. Gruendl, K. Zogal, P. Debernardi, C. Gier, C. Grasse, K. Geiger, R. Meyer, G. Boehm, M.-C. Amann, P. Meissner, and F. Kueppers, "50 nm continuously tunable MEMS VCSEL devices with surface micromachining operating at 1.95 μm emission wavelength", *Semicond. Sci. Technol.* 28 (1), 012001 (2012).

[8] L.S. Rothman, I.E. Gordon, A. Barbe, D.C. Benner, P.F. Bernath, M. Birk, V. Boudon, L.R. Brown, A. Campargue, J.-P. Champion, K. Chance, L.H. Coudert, V. Dana, V.M. Devi, S. Fally, J.-M. Flaud, R.R. Gamache, A. Goldman, D. Jacquemart, I. Kleiner, N. Lacome, W.J. Lafferty, J.-Y. Mandin, S.T. Massie, S.N. Mikhailenko, C.E. Miller, N. Moazzen-Ahmadi, O.V. Naumenko, A.V. Nikitin, J. Orphal, V.I. Perevalov, A. Perrin, A. Predoi-Cross, C.P. Rinsland, M. Rotger, M. Šimečková, M.A.H. Smith, K. Sung, S.A. Tashkun, J. Tennyson, R.A. Toth, A.C. Vandaele, and J. Vander Auwera, "The HITRAN 2008 molecular spectroscopic database", *J. Quant. Spectrosc. Radiat. Transfer* 110 (9–10) 533–572 (2009).

[9] S. Arafin, A. Bachmann, K. Vizbaras, and M.C. Amann, "Large-aperture single-mode GaSb-based BTJ-VCSELs at 2.62 μm", *22nd IEEE Int. Semiconductor Laser Conf. (ISLC)* 1, 47–48 (2010).

[10] A. Joullié, P. Christol, A.N. Baranov, and A. Vicet, "Mid-infrared 2–5 μm heterojunction laser diodes", in *Solid-State Mid-Infrared Laser Sources, Topics Appl. Phys.*, ed. I.T. Sorokina, K.L. Vodopyanov vol. 89, pp. 1–61, Springer-Verlag, Berlin, 2003.

[11] S. Adachi, *Properties of Semiconductor Alloys: Group-IV, III-V and II-VI Semiconductors*, John Wiley & Sons, Chichester, 2009.

[12] R.P. Sarzała, Ł. Piskorski, P. Szczerbiak, R. Kudrawiec, and W. Nakwaski, "An attempt to design long-wavelength (>2 μm) InP-based GaInNAs diode lasers", *Appl. Phys.* A 108 (3), 521–528 (2012).

[13] G.L. Bir and G.E. Pikus, *Symmetry and Strain-induced Effects in Semiconductors*, Wiley, New York, 1974.

[14] G.P. Donati, R. Kaspi, and K.J. Malloy, "Interpolating semiconductor alloy parameters: Application to quaternary III–V band gaps", *J. Appl. Phys.* 94 (9), 5814–5819 (2003).

[15] I. Vurgaftman, J.R. Meyer, and L.R. Ram-Mohan, "Band parameters for III-V compound semiconductors and their alloys", *J. Appl. Phys.* 89 (11), 5815–5875 (2001).

[16] I. Vurgaftman and J.R. Meyer, "Band parameters for nitrogen-containing semiconductors", *J. Appl. Phys.* 94 (6), 3675–3696 (2003).

[17] S.L. Chuang, *Physics of Optoelectronic Devices*, Wiley, Chichester, 1995.

[18] M. Bugajski, "Optical gain in quantum well lasers including many-body effects", *Electron Technol.* 30 (2), 89–98 (1997).

[19] R.P. Sarzała, M. Wasiak, T. Czyszanowski, and W. Nakwaski, "Performance characteristics of the 1.3-μm oxide-confined edge-emitting quantum-dot (InGa)As/GaAs diode lasers", *Bull. Pol. Ac.: Tech.* 52 (3), 257–263 (2004).

[20] L.C. Lew Yan Voon and M. Willatzen, *The k·p Method: Electronic Properties of Semiconductors*, Springer-Verlag, Berlin, 2009.

[21] P.G. Eliseev, "Line shape function for semiconductor laser modeling", *Electron. Lett.* 33 (24), 2046–2048 (1997).

[22] R. Kudrawiec, "Alloying of GaN_xAs_{1-x} with InN_xAs_{1-x}: a simple formula for the bandgap parametrization of $Ga_{1-y}In_yN_xAs_{1-x}$ alloys", *J. Appl. Phys.* 101 (2), 023522 (2007).

[23] R.P. Sarzała, P. Szczerbiak, and R. Kudrawiec, "Lasers with active regions of diluted nitrides on InP substrate emitting within a range of middle infrared", *Electronics* 10, 82–84 (2011), (in Polish).

[24] Ł. Piskorski and R.P. Sarzała, "GaInNAs quantum-well vertical-cavity surface-emitting lasers emitting at 2.33 μm", *Bull. Pol. Ac.: Tech.* 61 (3), 737–744 (2013).

[25] R.P. Sarzała, Ł. Piskorski, R. Kudrawiec, and W. Nakwaski, "Optimization of GaInNAs quantum-well vertical-cavity surface-emitting laser emitting at 2.33 μm", *Appl. Phys*. A 115 (3), 961–969 (2014).

[26] Ł. Piskorski, L. Frasunkiewicz, A.K. Sokół, and R.P. Sarzała, "A possibility to achieve emission in the mid-infrared wavelength range from semiconductor laser active regions", *16th Int. Conf. Transparent Optical Networks (ICTON)* We.P.9, 9 (2014).

[27] Z.Q. Li and Z.M. Simon Li, "Comprehensive analysis of GaSb-based mid-infrared vertical-cavity surface-emitting lasers", *Proc. SPIE* 8639, 863907 (2013).

[28] T. Czyszanowski, "Thermal properties and wavelength analysis of telecom oriented photonic-crystal VCSELs", *Opto-Electron. Rev.* 18 (1), 56–62 (2010).

[29] O. Dier, S. Dachs, M. Grau, L. Chun, C. Lauer, and M.-C. Amann, "Effects of thermal annealing on the band gap of GaInAsSb", *Appl. Phys.* A 86 (15), 151120 (2005).